Structural Basis of Substrate Recognition by Hematopoietic Tyrosine Phosphatase[†,‡]

David A. Critton,[§] Antoni Tortajada,[§] Geoffrey Stetson,[§] Wolfgang Peti,[‖] and Rebecca Page*,[§]

Departments of Molecular Biology, Cell Biology, and Biochemistry and of Molecular Pharmacology, Physiology, and Biotechnology, Brown University, Providence, Rhode Island 02912

Received September 9, 2008; Revised Manuscript Received October 23, 2008

ABSTRACT: Hematopoietic tyrosine phosphatase (HePTP) is one of three members of the *k*inase *i*nteraction *m*otif (KIM) phosphatase family which also includes STEP and PCPTP1. The KIM-PTPs are characterized by a 15 residue sequence, the KIM, which confers specific high-affinity binding to their only known substrates, the MAP kinases Erk and p38, an interaction which is critical for their ability to regulate processes such as T cell differentiation (HePTP) and neuronal signaling (STEP). The KIM-PTPs are also characterized by a unique set of residues in their PTP substrate binding loops, where 4 of the 13 residues are differentially conserved among the KIM-PTPs as compared to more than 30 other class I PTPs. One of these residues, T106 in HePTP, is either an aspartate or asparagine in nearly every other PTP. Using multiple techniques, we investigate the role of these KIM-PTP specific residues in order to elucidate the molecular basis of substrate recognition by HePTP. First, we used NMR spectroscopy to show that Erk2-derived peptides interact specifically with HePTP at the active site. Next, to reveal the molecular details of this interaction, we solved the high-resolution three-dimensional structures of two distinct HePTP−Erk2 peptide complexes. Strikingly, we were only able to obtain crystals of these transient complexes using a KIM-PTP specific substrate-trapping mutant, in which the KIM-PTP specific residue T106 was mutated to an aspartic acid (T106D). The introduced aspartate side chain facilitates the coordination of the bound peptides, thereby stabilizing the active dephosphorylation complex. These structures establish the essential role of HePTP T106 in restricting HePTP specificity to only those substrates which are able to interact with KIM-PTPs via the KIM (e.g., Erk2, p38). Finally, we describe how this interaction of the KIM is sufficient for overcoming the otherwise weak interaction at the active site of KIM-PTPs.

Tyrosine phosphorylation is a key mechanism for signal transduction and the regulation of an extensive set of physiological processes characteristic of multicellular organisms (*1*). Its importance is also well illustrated by the many inherited or acquired human diseases that stem from abnormalities in protein tyrosine phosphatases (PTPs) and protein tyrosine kinases (PTKs) (*2−4*). Hematopoietic tyrosine phosphatase (HePTP) (*5, 6*) is a small class I nonreceptor PTP which is expressed exclusively in the immune system,

especially T cells (*5−7*). It has a molecular mass of 38 kDa and consists of a catalytic PTP domain with a short (∼45 residues) N-terminal extension. The phosphatase activity of HePTP negatively regulates T cell activation and proliferation, as studies have shown that transient expression of HePTP in T cells causes a clear reduction in TCR-induced transcriptional activation (*8*). This is mediated via regulation of its only known physiological substrates, the mitogen-activated protein (MAP) kinases Erk1, Erk2, and p38 (*8−12*). These substrates bind HePTP via a 15 amino acid sequence, the *k*inase *i*nteraction *m*otif (KIM), within the HePTP N-terminus.

HePTP is one of three members of the KIM-containing family of PTPs, which also includes the striatal enriched phosphatase (STEP) and PC12 protein tyrosine phosphatase (PCPTP1). Primary sequence comparison of the KIM-phosphatase family with more than 30 other class I PTPs (*13*) reveals one region that is unique to the KIM-phosphatases: the PTP substrate binding loop (SBL). The KIM-phosphatases contain four residues in the SBL that are specific only to this family while, in other PTPs, these residues are highly conserved in and of themselves (Figure 1). The KIM-phosphatase conserved residues are H(L)98, T106, N110, and P111 (HePTP numbering). While H(L)98, N110, and P111 are located at the periphery of the SBL, T106 is in close proximity to the active site (*14, 15*). Notably, nearly every other PTP contains an aspartate, glutamate, or

‡ Atomic coordinates for HePTP−peptide complexes determined using X-ray crystallography have been deposited with the Protein Data Bank as entries 3D42 and 3D44.
* To whom correspondence should be addressed: phone, 401-863-6076; fax, 401-863-9653; e-mail, rebecca_page@brown.edu.
§ Department of Molecular Biology, Cell Biology and Biochemistry, Brown University.
‖ Department of Molecular Pharmacology, Physiology and Biotechnology, Brown University.

	98							106				111		
HePTP, STEP, PCPTP1	HI	X	X	K N R Y	K	T	I	L	P	N	P		
CD45	N	Q	N	K N R Y	V	D	I	L	P	Y	D		
RPTPs μ, κ, ρ	N	R	X	K N R Y	G	N	I	I	AS	Y	D		
LAR, RPTPs σ, δ	N	K	P	K N R Y	A	N	V	I	A	Y	D		
RPTPs α, ε	N	KRE	K N R Y	VP	N	I	L	P	Y	ND			
RPTPs γ, ζ	N	K	H	K N R Y	I	N	I	LV	A	Y	D		
RPTPβ, DEP1, SAP1, GLEPP	N	RN	X	K N R Y	X	N	IV	L	P	Y	D		
PTP1B, TCPTP	N	KR	N	R N R Y	R	D	V	S	P	FY	D		
PTPH1, PTP-MEG1	N	IL	X	K N R Y	RK	D	IVSL	P	Y	D			
PTPD1, PTPD2	N	A	E	R NS R	X X	DE	V	LV	P	Y	DE		
PTP-BAS	N	R	R	K N R Y	K	N	I	L	P	Y	D		
SHP1, SHP2	N	K	X	K N R Y	K	N	I	L	P	F	D		
PTP-MEG2	N	L	E	K N R Y	G	D	V	P	C	L	D		
Lyp, PTP-PEST	N	VI	K	K N R Y	K	D	I	L	P	FY	D		
HD-PTP	Y	S	L	K N R H	Q	D	V	M	P	Y	D		

FIGURE 1: The family of KIM-containing phosphatases have a unique PTP substrate binding loop. Consensus sequence alignment of 15 human PTP families. Similar amino acids are shaded in light gray. Members of the KIM-phosphatase family, including HePTP, are in dark gray, and the residue numbers above the alignment correspond to HePTP numbering. Residues of the PTP substrate binding loop specific to the KIM-phosphatase family are boxed and correspond to HePTP residues H98, T106, N110, and P111. The sequences used for this analysis are described in ref *13*.

asparagine at the equivalent position (e.g., in PTP1B, this residue is an aspartate) (*13*).

Using a variety of techniques, we have investigated the role of these KIM-phosphatase specific residues in order to elucidate the molecular basis of substrate recognition and dephosphorylation by HePTP. First, we used NMR spectroscopy to show that phosphorylated Erk2-derived peptides interact specifically with HePTP at the active site. Next, in order to understand the molecular basis for Erk2 peptide binding and specificity, we determined the high-resolution crystal structures of HePTP bound to two distinct Erk2 peptide substrates: a monophosphorylated Erk2 peptide and a dually phosphorylated Erk2 peptide mimetic. These represent the first crystal structures of a KIM-phosphatase in complex with substrate peptides. Our structures show, for the first time, that the interactions at the active site between KIM-phosphatases and their substrates are predominantly nonspecific, with the majority of the KIM-phosphatase residues coordinating the peptide backbone rather than residue side chains. These structures also illustrate that the KIM-phosphatase conserved residue T106 (Figure 1) likely functions to prevent HePTP from promiscuously binding tyrosine-phosphorylated proteins. Together, these results suggest that substrate specificity is mediated predominantly by residues distal from the active site, especially the KIM. Finally, we describe how the interaction provided by the KIM is sufficient for overcoming the otherwise weak interaction at the active site of KIM-phosphatases. These studies provide the first structural insights into the molecular basis of substrate recognition and dephosphorylation by HePTP and the KIM-phosphatase family.

MATERIALS AND METHODS

Cloning and Mutagenesis. Molecular cloning was carried out using standard protocols. The open reading frame of HePTP$_{44-339}$ was cloned into a derivative of the pBAD bacterial expression vector (Invitrogen), pMH1 (*16*), which contains an N-terminal expression and hexahistidine purification tag (MGSDKIHHHHHHM) or a derivative of pET28a

(Novagen) with the same tag (*17*). HePTP$_{15-339}$ was cloned into pET30a using a C-terminal primer that incorporated a hexahistidine tag at the C-terminus of HePTP. Mutagenesis was carried out using the QuikChange mutagenesis kit (Stratagene) following the enclosed protocols. All constructs were verified by sequencing (SeqWright).

Protein Expression and Purification. HePTP constructs (wild type and mutants) were typically expressed and purified as follows. For unlabeled protein, the appropriate expression plasmid was transformed into BL21-CodonPlus (DE3)-RIL (Stratagene) cells and expression carried out in LB medium containing appropriate antibiotics. To prepare ^{2}H,^{15}N-labeled protein, *Escherichia coli* BL21-CodonPlus (DE3)-RIL (Stratagene) cells transformed with the HePTP expression plasmid were grown in M9 minimal medium containing [^{2}H, 99.8%]deuterium oxide and [^{15}N, 99%]ammonium chloride (CIL), as well as appropriate antibiotics. Cell cultures were grown at 37 °C with vigorous shaking to an OD$_{600}$ of 0.5−0.9, at which point the cells were transferred to 4 °C and the shaker temperature was lowered to 18 °C. Expression was induced by the addition of either 0.02% L-arabinose or 1 mM IPTG (final concentrations) as appropriate, and the cultures were grown for an additional 18 h at 18 °C with vigorous shaking. The cells were harvested by centrifugation and resuspended in extraction buffer (50 mM Tris, pH 8.0, 500 mM NaCl, 5 mM imidazole, 0.1% Triton X-100, and EDTA-free protease inhibitor tablets; Roche) and lysed by high-pressure cell homogenization (Avestin C3 Emulsiflex). The cell debris was removed by centrifugation (35000*g* for 35 min at 4 °C). The filtered supernatant was loaded onto a HisTrap HP column (GE Healthcare) equilibrated with 50 mM Tris, pH 8.0, 5 mM imidazole, and 500 mM NaCl and eluted with a 5−300 mM imidazole gradient. Purified fractions were pooled and dialyzed against protein buffer (10 mM Tris, pH 7.8, 100 mM NaCl, 0.5 mM TCEP). After concentration, the proteins were further purified using size exclusion chromatography (Superdex75 26/60; GE Healthcare) equilibrated in protein buffer. Fractions corresponding to monomeric protein were pooled, concentrated, and either used immediately or frozen in liquid nitrogen and stored at −80 °C until needed. Fractions corresponding to monomeric, labeled protein for NMR experiments were pooled, concentrated, and used immediately. Erk2 was expressed and purified following described protocols (*18*).

Peptides. All peptides used in this study were synthesized and HPLC-purified by Biosynthesis Inc. The molecular masses of all peptides were verified by mass spectrometry. Peptides were obtained as a lyophilized powder and were reconstituted in protein buffer to final concentrations of 10 mM. Peptide solutions were either used immediately or stored at −20 °C and thawed immediately before use.

Michaelis−Menten Kinetic Assay. The general PTP substrate *p*-nitrophenyl phosphate (*p*NPP) was purchased from Sigma. All other chemicals and reagents were of the highest grade commercially available. The HePTP-catalyzed hydrolysis of *p*NPP was assayed at 30 °C in 0.15 M Bis-Tris, pH 6.0, with ionic strength adjusted to 150 mM with NaCl. The reaction was initiated by addition of various concentrations of *p*NPP (ranging from 0.1 to 5 K_m) to the reaction mixture to a final volume of 100 μL. The reaction was quenched by addition of 100 μL of 1 M NaOH. The nonenzymatic hydrolysis of the substrate was corrected by

measuring the control without addition of enzyme. The amount of p-nitrophenolate product was determined from the absorbance at 405 nm detected by a microplate reader (SpectraMax M5, Molecular Devices, or PowerWaveX340, Bio-Tek Instruments), using a molar extinction coefficient of 18000 M^{-1} cm^{-1}. The Michaelis−Menten constant (K_m) and turnover number (k_{cat}) were evaluated by fitting the data to the Michaelis−Menten equation, using nonlinear regression and the program SigmaPlot (version 8.0).

NMR Spectroscopy. NMR experiments were performed at 25 °C on a Bruker AVANCE II 800 MHz spectrometer equipped with a 5 mm TCI [HCN] z-gradient cryoprobe. All data were processed and evaluated using Topspin 1.3 (Bruker). All HePTP−ligand interaction experiments were carried out using the wild-type HePTP catalytic domain: WT-HePTP$_{44-339}$. 2D [^{1}H,^{15}N] TROSY-based NMR experiments (19) for WT-HePTP$_{44-339}$ were performed at a protein concentration of 0.5 mM in NMR buffer (10 mM Tris, pH 7.8, 100 mM NaCl, 10% (v/v) D_2O); experiments for HePTP titrated with phosphotyrosine (Sigma-Aldrich) were performed at a protein concentration of 0.5 mM in NMR buffer and titrated with equimolar and a 4-fold excess of pY; experiments for the HePTP−peptide complex were performed at a protein concentration of 0.5 mM in NMR buffer, titrated with a 3-fold excess of dually phosphorylated Erk2 peptide mimetic ^{182}LpTEsYVATR^{189} (sY, sulfonated tyrosine).

Crystallization. Proteins were crystallized using the sitting drop vapor diffusion method at 4 °C. HePTP$_{44-339}$ C270S/T106D was incubated with a 3-fold molar excess of the monophosphorylated Erk2 peptide ^{182}LTEpYVATR^{189} for 30 min at 4 °C, after which precipitate was separated from the soluble complex by centrifugation. Crystals were obtained in 0.2 M ammonium tartrate, pH 6.6, and 20% (w/v) PEG 3350 and cryoprotected in 20% (v/v) glycerol containing 2 mM peptide (direct soak, 0.5 min) prior to diffraction screening and data collection. HePTP$_{44-339}$ C270S/T106D was incubated with a 3-fold molar excess of the dually phosphorylated Erk2 peptide mimetic ^{182}LDEpYVATR^{189} for 30 min at 4 °C, after which the precipitate was separated from the soluble complex by centrifugation. Crystals were obtained in 1.0 M lithium chloride, 0.1 M citrate, pH 5.0, and 20% (w/v) PEG 6000 and were cryoprotected in 20% (v/v) glycerol containing 2 mM peptide (direct soak, 1 min) prior to diffraction screening and data collection.

Data Collection and Structure Determination. Data for both HePTP T106D/C270S−Erk2 peptide complexes were collected at Brookhaven National Laboratory National Synchroton Light Source (BNL-NSLS) beamline X6A at 100 K using an ADSC QUANTUM 210 CCD detector. Data were indexed, scaled, and merged using HKL2000 0.98.692i (20). Structures were solved by molecular replacement using the program Phaser 1.3.2 (21) and the structure of the HePTP catalytic domain D236A/C270S/Q314A mutant (PDB code 2QDM) as a search model, after omitting solvent molecules. The resulting rotation- and translation-function Z-scores were >35 for both data sets. Models were completed by cycles of manual building using the program Coot 6.0.2 (22) coupled with structure refinement using RefMac 5.2.0019 (23) against the native data sets. The structure of the HePTP T106D/C270S−Erk2 peptide LTEpYVATR complex was determined to 2.45 Å resolution and refined to an R factor

of 18.1% (R_{free} = 24.1%), and contains HePTP residues 44−335, peptide residues 183−186, and 118 water molecules (HePTP residues 178−180, 336−339, and peptide residues 182, 187−189 were not observed in the electron density map). The structure of the HePTP T106D/C270S−Erk2 peptide LDEpYVATR complex was determined to 1.9 Å resolution and refined to an R factor of 16.4% (R_{free} = 20.4%) and contains HePTP residues 44−335, peptide residues 183−186, and 271 water molecules (HePTP residues 122−124, 178−182, 336−339 and peptide residues 182, 187−189 were not observed in the electron density map). The stereochemical quality of each model was analyzed using MolProbity (24), which performs Ramachandran plot, Cβ deviation, and rotamer analyses. The agreement of each model to the diffraction data was analyzed using SFCheck 7.2.02 (25). Atomic coordinates and structure factors for the HePTP−Erk2 peptide complexes determined using X-ray crystallography have been deposited with the Protein Data Bank as entries 3D42 and 3D44.

Isothermal Titration Calorimetry. ITC experiments were performed at 25 °C using a VP-ITC microcalorimeter (Microcal Inc.). HePTP$_{15-339}$ (titrant; 566 μM) in 10 mM Tris, pH 7.8, 100 mM NaCl, and 0.5 mM TCEP was titrated into 35 μM Erk2 (cell sample) in the same buffer. The solution in the cell was stirred at 307 rpm by the syringe to ensure rapid mixing. Titrant (10 μL per injection) was delivered over 63 min with an adequate interval (250 s) between injections to allow complete equilibration. Data were collected automatically and analyzed with a one-site binding model using Origin 7.0. Origin uses a nonlinear least-squares algorithm (minimization of χ^2) and the concentrations of the titrant and the sample to fit the heat flow per injection to an equilibrium binding equation, providing values of the stoichiometry (n), change in enthalpy ($\Delta H°$), and binding constant (K).

RESULTS

Erk2 Peptide Substrate Mimetics Interact with HePTP at the Active Site. We used NMR spectroscopy to verify that the family of Erk2 peptides used in this study, which are considerably shorter than those used in previous kinetic studies of HePTP (26), interacts at the HePTP active site. For these experiments, a representative Erk2 peptide that mimics the Erk2 dually phosphorylated state (^{182}LpTEsY-VATR^{189}) was used. Three 2D [^{1}H,^{15}N] TROSY spectra of ^{2}H,^{15}N-labeled WT HePTP$_{44-339}$ were collected: (1) 0.5 mM HePTP$_{44-339}$ alone (Figure 2A); (2) 0.5 mM HePTP$_{44-339}$ in the presence of an equimolar and a 4-fold excess of phosphotyrosine (Figure 2B); and (3) 0.5 mM HePTP$_{44-339}$ in the presence of a 3-fold excess of freshly prepared peptide (the same ratio as that used for subsequent crystallization trials; Figure 2C). The locations of peaks that shift upon titration with phosphotyrosine are highlighted with black circles (Figure 2B) and, based on the conserved catalytic mechanism of PTPs, likely correspond to residues at the HePTP active site. As can be seen in Figure 2C, these same peaks shift upon addition of the Erk2 peptide (black circles), indicating that the Erk2 peptide also interacts at the active site. Furthermore, a few additional peaks shift in the presence of peptide (gray circles), demonstrating that only a few residues outside the active site participate in substrate
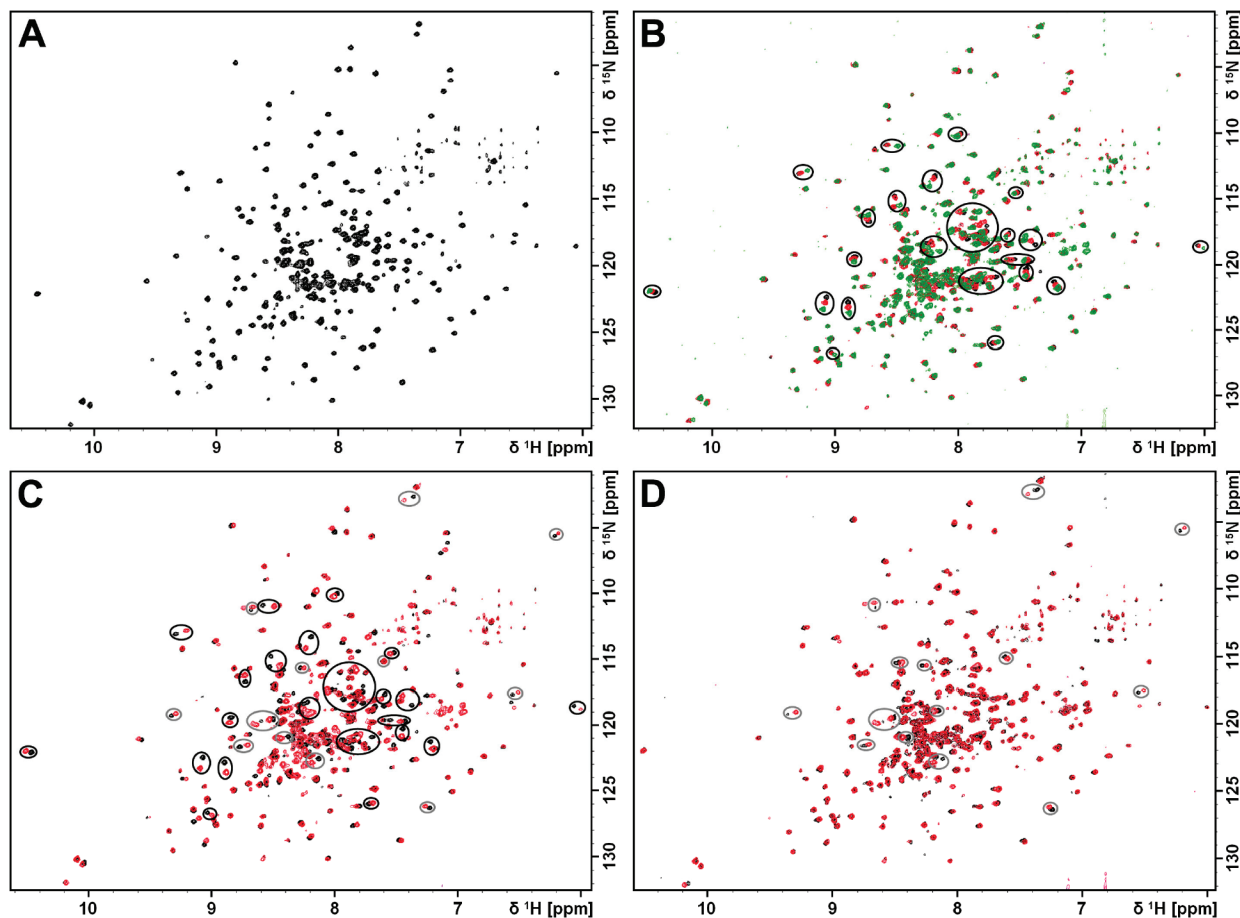
FIGURE 2: Erk2 peptide ^{182}LpTEsYVATR^{189} binds at the HePTP active site. (A) The two-dimensional correlation spectrum for HePTP is well resolved, and nearly all individual peaks can be distinguished, allowing for straightforward detection of chemical shift changes upon ligand interaction. 2D [^{1}H,^{15}N] TROSY spectrum for ^{2}H,^{15}N-labeled HePTP$_{44-339}$ (0.5 mM) recorded at 25 °C on a Bruker Avance II 800 MHz spectrometer. (B) The locations of peaks corresponding to residues at the HePTP active site were determined by titrating the sample with phosphotyrosine. The 2D [^{1}H,^{15}N] TROSY spectra for ^{2}H,^{15}N-labeled HePTP$_{44-339}$ (0.5 mM; black), ^{2}H,^{15}N-labeled HePTP$_{44-339}$ titrated with 0.5 mM phosphotyrosine (red), and ^{2}H,^{15}N-labeled HePTP$_{44-339}$ titrated with 2 mM phosphotyrosine (green) are shown. The locations of those peaks that shift upon interaction with phosphotyrosine are highlighted with black circles. (C) The 2D [^{1}H,^{15}N] TROSY spectrum for ^{2}H,^{15}N-labeled HePTP$_{44-339}$ (0.5 mM; black) and ^{2}H,^{15}N-labeled HePTP$_{44-339}$ titrated with 1.5 mM freshly prepared Erk2 peptide (^{182}L*p*TE*s*YVATR^{189}; red). The locations of those peaks that shift upon interaction with peptide are highlighted with circles (black circles, peaks that also shift upon titration with *p*Y; gray circles, peaks that shift only in the presence of peptide). (D) Superposition of the 2 mM phosphotyrosine-titrated spectrum from (B) (black) with the 1.5 mM peptide-titrated spectrum from (C) (red) to more clearly illustrate the additional peak shifts observed due to peptide binding (gray circles, peaks that shift only in the presence of peptide).

binding. The peaks that shift exclusively upon the addition of peptide are highlighted in Figure 2D, where the spectra from the HePTP−*p*Y (1:4 protein:*p*Y ratio; black) and HePTP−Erk2 peptide (1:3 protein:peptide ratio, red) complexes are superimposed.

Biochemical Characterization of HePTP Substrate-Trapping Mutants. In order to obtain crystals of HePTP in complex with phosphorylated Erk2 peptides, multiple HePTP substrate-trapping mutants (STMs) of the HePTP catalytic domain (HePTP residues 44−339) were generated. These include seven "canonical" STMs (four single mutants, D236A, C270S, C270A, Q314A; one double mutant, D236A/Q314A; two triple mutants, D236A/C270S/Q314A, D236A/C270A/Q314A) and a "KIM-phosphatase specific" STM (T106D/C270S). All proteins were produced in *E. coli*. The thermal stability and structural integrity of the produced proteins were verified by CD polarimetry and, in some cases, by structure determination (Supporting Information Figure S1).

The kinetic parameters for WT and mutant HePTP-catalyzed hydrolysis of *p*NPP were determined and are

Table 1: Kinetic Parameters of the HePTP$_{44-339}$ Catalytic WT- and Substrate-Trapping Mutant- (STM-) Catalyzed Dephosphorylation of pNPP[a]

protein	k_{cat} (s^{-1})	K_m (mM)	k_{cat}/K_m (M^{-1} s^{-1})
HePTP$_{44-339}$			
WT	12.55 ± 0.12	3.26 ± 0.07	3849.69
Canonical STMs			
Q314A	0.93 ± 0.02	2.11 ± 0.10	440.08
D236A	0.03 ± 0.00	1.31 ± 0.07	22.9
D236A/Q314A	0.01 ± 0.00	0.56 ± 0.01	17.85
C270S	ND[b]	ND	ND
C270S/D236A/Q314A	ND	ND	ND
C270A	ND	ND	ND
C270A/D236A/Q314A	ND	ND	ND
KIM-Phosphatase Specific STM			
C270S/T106D	ND	ND	ND

[a] STMs listed in order of decreasing catalytic efficiency. [b] ND: no detectable activities observed for these mutants.

summarized in Table 1. The mutation of the Q-loop glutamine to an alanine (Q314A) had the smallest effect on HePTP catalytic activity, with an observed k_{cat} of 0.93 s^{-1}, only 13-fold lower than that of WT-HePTP. Mutation of the

catalytic aspartate of the WPD loop to an alanine (D236A) had the next largest effect on k_{cat}, which was reduced by an additional order of magnitude to 0.03 s^{-1}, 420-fold lower than that of WT. The combination of these two mutations (D236A/Q314A) resulted in a mutant with a k_{cat} lower than that of D236A alone (0.01 s^{-1}), making it 1255-fold less active than WT. This mutant also had a modestly lower K_m than both single mutants and WT, with a K_m 5-fold lower than that of WT. This modest change in K_m upon mutation of HePTP active site residues contrasts to what has been observed for PTP1B. The simultaneous mutation of the corresponding residues in PTP1B (D181A/Q262A) causes the K_m for pNPP hydrolysis to decrease by a full 2 orders of magnitude, from 2.4 to 0.024 mM (*27*). This suggests that the active site microenvironment of the HePTP differs from that of PTP1B. Finally, mutation of the catalytic site nucleophilic cysteine to either serine or alanine (C270S or C270A) alone (single mutants) or in combination with other mutations (triple mutants; KIM-phosphatase specific mutant) produced the most dramatic effect, with catalytic activities that were too low be accurately measured.

Structure Determination of the HePTP−Erk2 Peptide Complexes. In an effort crystallize a catalytically inactive HePTP mutant in complex with monophosphorylated and dually phosphorylated Erk2 peptides, several HePTP STMs and Erk2 peptides were used. In spite of extensive efforts using canonical HePTP STMs (Supporting Information Figure S1), diffraction quality crystals of the HePTP−Erk2 peptide complexes were obtained only with the KIM-phosphatase specific STM, HePTP$_{44−339}$ T106D/C270S. Thus, although Erk2 peptides clearly interact with HePTP at the active site (Figure 2), the complexes formed were not sufficiently stable to support crystal formation unless the HePTP T106D mutation was present.

We determined the high-resolution structures of HePTP in complex with two distinct Erk2 peptides: (1) ^{182}LTEpY-VATR^{189}, an eight-residue peptide that corresponds to the monophosphorylated Erk2 activation loop, and (2) ^{182}LDEpY-VATR^{189}, an eight-residue peptide that corresponds to the dually phosphorylated Erk2 activation loop (the T183D mutation in the peptide provides a carboxylate group that emulates phosphothreonine) (*28, 29*). The structure of the HePTP−^{182}LTEpYVATR^{189} peptide complex, referred to hereafter as the monophosphorylated complex, was determined to 2.45 Å resolution and refined to an *R* factor of 18.1% (R_{free} = 24.1%). The structure of the HePTP−^{182}LDEpYVATR^{189} peptide complex, referred to hereafter as the dually phosphorylated complex, was determined to 1.9 Å resolution and refined to an *R* factor of 16.4% (R_{free} = 20.4%).

Both structures are illustrated in Figure 3A. As can be seen from Figure 3B,C, electron density for the Erk2 peptides is clearly visible. The strongest density is observed for the phosphotyrosine moiety, pY185, which is bound at the HePTP active site. While electron density is observed for residues immediately N- and C-terminal to the central pY185, electron density for residues at the peptide termini is not observed, suggesting these terminal residues are disordered in the crystal. Thus, residues L182, A187, T188, and R189 of both peptides were not modeled. The residues of both peptides that are visible (residues 183−186) were refined

with occupancies of 1.0. Data statistics for both structures are summarized in Table 2.

Erk2 Residue T183, Which Is Phosphorylated in Maximally Activated Erk2, Is Not Essential for Substrate Recognition and Binding by HePTP. The structures of the two HePTP−peptide complexes show that both peptides bind HePTP via similar interactions (Figure 3A). In particular, there are no differences in the way that peptide residue 183, which is a threonine in the monophosphorylated structure and a pT-emulating aspartate in the dually phosphorylated structure, interacts with HePTP. In addition, electron density for the side chain of this peptide residue is weak in both structures. These observations suggest that Erk2 residue 183 does not form strong interactions with any residues from HePTP, either in its unphosphorylated or phosphorylated state, and thus that the additional negative charge on the pT-emulating peptide (^{182}LDEpYVATR^{189}) does not contribute to binding. This provides a structural explanation for the observation that monophosphorylated (pY185) and dually phosphorylated (pT183/pY185) Erk2 are dephosphorylated by HePTP with similar catalytic efficiencies (*26*). Because both peptides bind HePTP via essentially identical interactions, the remainder of this report discusses only the higher resolution, dually phosphorylated peptide complex.

HePTP Binds the Phosphorylated Tyrosine of the Erk2 Peptide (pY185) by a Conserved Network of Hydrogen Bonds. As can be seen from Figure 3D,E and Supporting Information Figure S2, the phosphorylated tyrosine of the Erk2 peptide, pY185, is anchored in the active site of HePTP by an extensive network of hydrogen-bonding interactions with residues of the PTP loop, similar to those observed in other PTP peptide- and phosphate-bound structures (*15, 30−34*). The main chain amide nitrogens of A272, I274, G275, and R276, along with the ϵ- and η-nitrogens of R276, form hydrogen bonds with the phosphate oxygens of pY185. pY185 is also anchored by aromatic interactions. The phenyl ring of pY185 forms an extended aromatic interaction with both the phenyl side chain of the conserved Y104 (located in the SBL; Figure 1) and the imidazole ring of H237 (located in the WPD loop, which is closed about the active site and thus in close proximity to the bound peptide). The geometries of these aromatic−aromatic interactions are comparable to those observed in other proteins (*35−39*), including PTPs (*30, 31*) (Supporting Information Table S2). Finally, HePTP residues ^{178}EGKEK^{182}, which we refer to as the E loop since HePTP residue E178 is 100% conserved among class I PTPs (*13*), are not observed in the HePTP−Erk2 peptide complexes. Comparison of this region with those of the other KIM-containing phosphatases (*14, 40*) clearly indicates that this region is highly flexible, as it is often disordered or, when visible, adopts a range of conformations with high *B*-factors (Supporting Information Figure S3).

The Backbone of the Erk2 Peptide Substrate Is Stabilized by Residues Outside of the PTP Loop. As can be seen from Figure 3D,E, residues outside the PTP loop of HePTP further stabilize the peptide backbone. First, the main chain amide nitrogen of HePTP residue K105 forms a hydrogen bond (3.1 Å) with the main chain carbonyl oxygen of peptide residue D183. Notably, the K105 side chain is only visible in the electron density map of the monophosphorylated HePTP−Erk2 peptide complex and, even when ordered, does not interact with the bound peptide. This is in contrast to
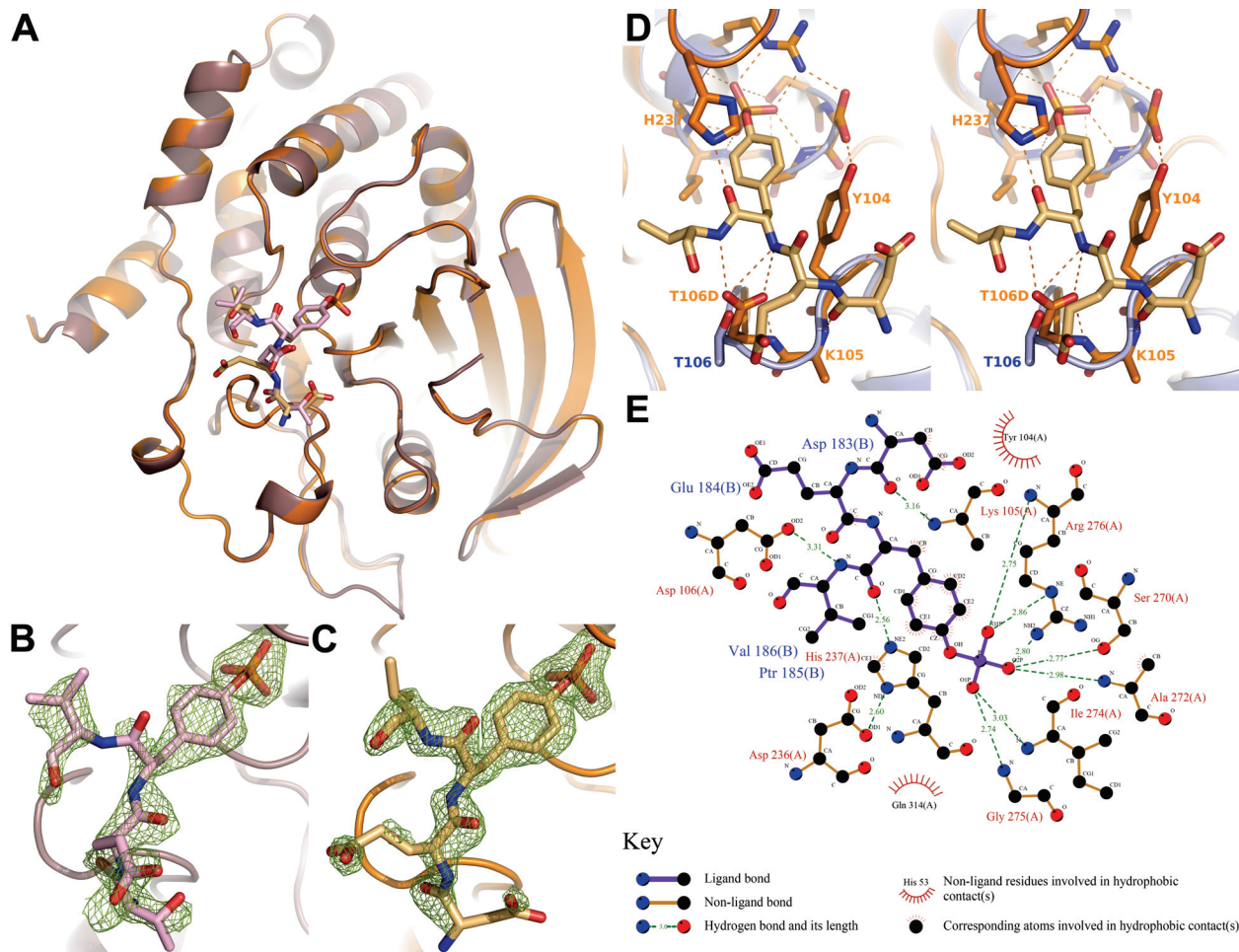
FIGURE 3: Erk2 substrate recognition by HePTP. (A) Superposition of the structures of HePTP$_{44-339}$ T106D/C270S bound to the Erk2 monophosphorylated peptide ([182]LTE*p*YVATR[189]; light purple) and dually phosphorylated peptide mimetic ([182]L*D*E*p*YVATR[189]; orange). The structures of both HePTP and the bound peptides are nearly identical (rmsd = 0.28 Å). (B, C) Sigma-A weighted $2mF_o - DF_c$ maps of (B) the Erk2 monophosphorylated peptide, refined at an occupancy of 1.0, and (C) dually phosphorylated peptide mimetic, refined at an occupancy of 1.0, bound to HePTP. Maps are contoured at 1.0σ to 2.45 and 1.9 Å, respectively. No electron density for peptide residues L182, A187, T188, and R189 was observed in either structure, and thus these residues were not modeled. Figures prepared using Pymol (*47*). (D) Stereo image of the superposition of the Erk2 dually phosphorylated peptide mimetic (light orange; stick representation) bound in the active site of HePTP T106D/C270S (dark orange; cartoon representation) superimposed onto apo-HePTP C270S (light blue; cartoon representation). Polar contacts between the peptide and HePTP are illustrated by dashed lines. HePTP T106D/C270S residues Y104, K105, T106D, and H237 are shown as stick figures and form hydrogen bonds and polar interactions with the Erk2 peptide backbone (the side chain of K105 was not visible in the electron density map). HePTP C270S residue T106 is also shown as a stick figure. Threonine, with its shorter, uncharged side chain, is incapable of making bipartite polar interactions with bound substrates akin to those observed between T106D and the bound peptide, demonstrating the role of T106 as a negative determinant of substrate specificity. (E) Hydrogen-bonding interactions stabilize the Erk2 peptide at the active site of HePTP. Schematic representation of the detailed interactions between the Erk2 peptide [182]L*D*E*p*YVATR[189] and HePTP T106D/C270S. Ligand in purple and HePTP in orange. Hydrogen bonds (green dashed lines) and hydrophobic contacts (red semicircles) are illustrated. Figure prepared using LIGPLOT (*48*).

what has been observed in other PTPs such as PTP1B where this residue is an arginine (R47). In these structures, the side chain of R47 interacts with bound substrates via both electrostatic and hydrophobic interactions and thus plays an important role in accommodating and coordinating a variety of peptide substrates (*33*). Since the side chain of K105 in HePTP does not make similar interactions with the Erk2 peptide, it likely does not contribute to HePTP substrate specificity. Notably, K105 is moderately conserved among human PTPs (27%) (*13*), and thus it will be interesting to see if this residue plays a different role in substrate recognition and binding for other PTPs.

A second residue that is important for coordinating the Erk2 peptide substrate at the HePTP active site is H237 (Figure 3D). Besides forming an aromatic interaction with the *p*Y185 phenyl ring, the ϵ-nitrogen of H237 also forms a

strong hydrogen bond (2.5 Å; Figure 3D) with the *p*Y185 main chain carbonyl oxygen, an interaction which has not previously been observed in any other PTP−peptide complex. Thus, both the aromatic interaction and the strong hydrogen bond formed between H237 and the peptide provide sufficient stabilization energy for maintaining the WPD loop in a closed conformation, thereby allowing the adjacent catalytic residue, D236, to be optimally positioned for participation in catalysis. Because this histidine is ∼60% conserved across human PTP domains (*13*), we expect this novel role for H237 in coordinating PTP substrates to be similarly conserved in other human PTPs.

T106 Negatively Regulates Substrate Binding at the Active Site. As can be seen from Figure 3D,E, the T106D mutation, as predicted, provides even further stabilization of the peptide

Table 2: Summary of Crystal Parameters, Data Collection, and Refinement Statistics for HePTP$_{44-339}$ T106D/C270S−Erk2 Peptide Complexes

	[182]LTEpYVATR[189]	[182]LDEpYVATR[189]
PDB code	3D42	3D44
space group	C2	C2
Unit-Cell Parameters		
a, b, c (Å)	118.5, 39.0, 83.7	119.1, 38.9, 83.7
α, β, γ (deg)	90.0, 124.6, 90.0	90.0, 124.9, 90.0
wavelength (Å)	1.000	1.000
resolution (Å)	50.0−2.45 (2.54−2.45)[a]	50.0−1.90 (1.97−1.90)[a]
Z (molecules per ASU)	1	1
total/unique reflections	199966/11129	263604/25161
completeness (%)	94.3 (88.2)[a]	99.9 (99.5)[a]
mean I/σ(I)	9.7 (3.9)[a]	12.9 (2.8)[a]
R_{sym}[b] on I	0.111 (0.221)[a]	0.102 (0.459)[a]
Model Refinement and Statistics		
resolution range	20.00−2.45	20.00−1.90
no. reflections (total)	11109	25125
no. reflections (test)[c]	524	1283
R_{cryst}[c]	0.181	0.164
R_{free}[d]	0.241	0.204
Stereochemical Parameters		
rmsd bonds (Å)	0.016	0.011
rmsd angles (deg)	1.75	1.29
residues in most favorable region of Ramachandran plot (%)	96.5	97.1
average B (Å²)	15.9	17.9

[a] Highest resolution shell. [b] $R_{sym} = \sum|I_i - \langle I_i\rangle|/\sum|I_i|$, where I_i is the scaled intensity of the *i*th measurement and $\langle I_i\rangle$ is the mean intensity for that reflection. [c] $R_{cryst} = \sum\||F_o| - |F_c|\|/\sum|F_o|$, where F_c and F_o are the calculated and observed structure factor amplitudes, respectively. [d] R_{free} = as for R_{cryst} but for 5.0% of the total reflections chosen at random and omitted from refinement.

backbone. The side chain δ-oxygens of D106 form polar interactions (3.3−3.4 Å) with the main chain amide nitrogens of peptide residues *p*Y185 and V186. A threonine, with its shorter uncharged side chain, is incapable of making comparable interactions (Figure 3D; the structure of HePTP C270S is shown in light blue, with T106 shown in ball-and-stick representation, and HePTP C270S/T106D shown in orange). In spite of numerous attempts, crystals of HePTP$_{44-339}$ C270S single or triple mutants (Table 1) in complex with either peptide did not form. This demonstrates that although these peptides interact extensively at the active site of WT HePTP, as we showed using TROSY-based NMR spectroscopy, the interaction is sufficiently transient that it precludes crystal formation unless the T106D mutation, which anchors the peptide backbone, is introduced.

DISCUSSION

These structures illustrate that residues surrounding the active site do not significantly contribute to substrate recognition by the KIM-phosphatases. In both the HePTP− Erk2 peptide complexes, only four of the eight peptide residues are observed in the electron density maps, and those that are observed are immediately adjacent to the tightly bound, highly ordered phosphorylated tyrosine (*p*Y185; observed residues 183−186). This is in sharp contrast to what has been observed for other PTP−peptide complexes, in which the bound peptides interact extensively with PTP residues contiguous with the active site, burying as much as 800 Å² of solvent-accessible surface area upon complex formation (*30−33, 41*). In addition, excluding the interactions made with *p*Y185, HePTP peptide binding residues interact

almost exclusively with the peptide backbone; no significant interactions with peptide side chains are observed in either of our structures. Thus, although these interactions contribute to binding, they do not confer substrate specificity. This observation is consistent with kinetic data showing that HePTP dephosphorylates a variety of tyrosine-phosphorylated peptides, including peptides derived from Erk2 (an endogenous substrate), p130^{Cas} (a YopH substrate), and epidermal growth factor receptor (a PTP1B substrate), with virtually equivalent catalytic efficiencies (*26*).

Furthermore, our structures illustrate how HePTP residue T106 functions, as previously predicted, as a negative determinant of substrate binding (*26*). Although substrate peptides unequivocally bind WT-HePTP at the active site (Figure 2), the interaction is sufficiently transient that crystal formation is precluded unless the T106D mutation, which stabilizes the protein−peptide interaction, is introduced (Figure 3). The importance of this SBL residue in substrate binding has also been demonstrated biochemically: the catalytic efficiency of HePTP for dephosphorylating tyrosine-phosphorylated peptides increases by 33-fold when T106 is mutated to an aspartate, while the catalytic efficiency of PTP1B for dephosphorylating the same peptides decreases by 26-fold when the equivalent SBL residue, D48, is mutated to threonine (*26*).

Because the T106D mutation has such a clear effect on catalytic efficiency and substrate binding, and because the mutation of threonine to aspartate is often used to emulate phosphorylated threonine (*28, 29*), we considered whether T106 might be phosphorylated *in vivo*. Notably, the residues immediately adjacent to T106 are nearly 100% conserved among the KIM-phosphatases (Figure 1). In addition, this sequence is consistent with the consensus phosphorylation sites for certain serine/threonine kinases (*42*). However, while a number of studies have demonstrated that the reversible phosphorylation of HePTP *in vivo* is critical for regulating its activity (e.g., at residues S23, T45, S72, and S225; *12, 43, 44*), T106 has yet to be identified as a *bona fide* target for phosphorylation.

Rather, T106 most likely functions to prevent HePTP from promiscuously binding tyrosine-phosphorylated proteins. Specificity for HePTP's only known substrates, Erk and p38, is thus provided predominantly by a second protein interaction site, the KIM, which is distal from the active site (Figure 4C). Using isothermal titration calorimetry, we determined the dissociation constant (K_d) between HePTP$_{15-339}$, which includes the KIM, and Erk2 to be 549 nM (Figure 4A,B). Thus, the otherwise weak interaction at the active site of the KIM-containing phosphatases, due to the presence of the conserved SBL threonine (Figure 1), is overcome by the much stronger interaction provided by the KIM, which increases the local concentration of specific MAPK substrates.

Regions of HePTP outside both the KIM and the active site also contribute to substrate binding during catalysis. This has been demonstrated both biochemically (*26*) and by our observation that the K_d of the HePTP protein for Erk2 (Figure 4A,B) is ~10-fold stronger than that of an HePTP KIM peptide (HePTP residues 16−31) for Erk2 (*45*). In order to identify which regions of HePTP further contribute to substrate binding, we docked, as rigid bodies, the structure of the HePTP−Erk2 peptide complex, the structure of Erk2 bound to a peptide representing the HePTP KIM peptide
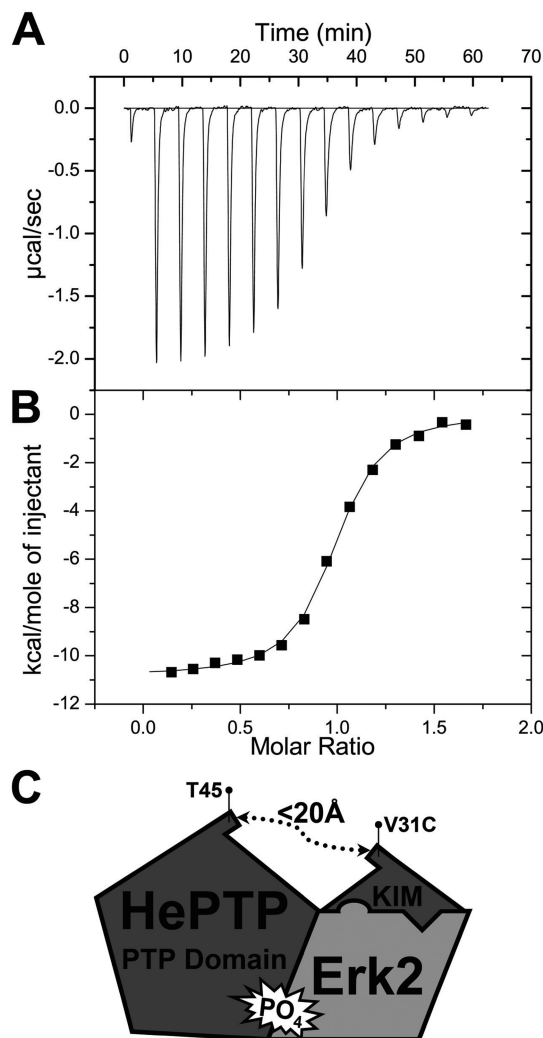
FIGURE 4: HePTP−Erk2 protein−protein interactions. Raw isothermal titration calorimetry data (A) and derived binding isotherm plotted vs the molar ratio of titrant fit using a one-site model (B) for 15 10-μL injections of HePTP$_{15-339}$ (which includes the HePTP KIM sequence, residues 15−31; 566 μM) into the isothermal cell containing the sample Erk2 (35 μM). The solid line in (B) is the best fit to the data using the nonlinear least-squares regression algorithm (ORIGIN). The calculated dissociation constant, K_d, is 549 ± 44 nM, the reaction stoichiometry, n, is 0.95 ± 0.01, and the change in enthalpy, ΔH, −10.8 kcal/mol. (C) Cartoon illustrating the HePTP−Erk2 dephosphorylation complex. The predicted distance between HePTP residues V31 and T45 is ∼16−20 Å, a distance easily traversed by the intervening 13 residues.

(HePTP residues 16−31; PDB code 2GPH (*45*)), and the structure of dually phosphorylated Erk2 (PDB code 2ERK (*46*)). Docking the coordinates of dually phosphorylated Erk2 onto the Erk2 peptide in the HePTP−Erk2 peptide complex (root-mean-square deviation of 1.7 Å) shows that Erk2 likely interacts with residues N-terminal to the SBL (HePTP residues Y104−L108). This rigid body docking results in steric clashes between HePTP and Erk2. However, the clashes are not excessive and are likely relieved by as yet undetermined conformational changes in both Erk2 (i.e., at the phosphorylation loop, which has been shown to adopt a range of conformations) and HePTP. Docking the KIM peptide from 2GPH also shows that the distance between T45 (the first residue of the HePTP catalytic domain) and V31C (the last residue of the KIM sequence) is ∼16.5 Å, a distance that is easily traversed by the intervening 13 residues

of HePTP. This interaction is illustrated in a cartoon representation (Figure 4C).

Based on our analysis, the N-terminal region of HePTP helix α0 (residues T45−A57) and the relatively long N-terminal coil region (residues V88−P111, which includes T106 and the SBL) are expected to be the regions of HePTP that interact most extensively with its bound MAPK substrates. The structure of this N-terminal coil region in the KIM-containing phosphatases is distinct from the conformations observed in other class I PTPs, such as PTP1B, Lyp, and CD45. This structural disparity is due to the presence of HePTP residue P111, which is conserved among the KIM-phosphatases while in nearly all other class I PTPs, the corresponding residue is an aspartate (Figure 1). In PTP1B, Lyp, and CD45, this aspartate (D53, D76, and D665, respectively) forms two hydrogen bonds with the main chain amide nitrogens from the N-terminal coil region. The KIM-phosphatases, which contain a proline at this position, are incapable of making comparable interactions and thus have structurally distinct, more flexible N-terminal coil regions. This is supported by the observation that this region adopts distinct conformations even within the KIM-phosphatase family (Supporting Information Figure S4). Thus, we expect HePTP, particularly at residues V88−P111, to adopt a novel, distinct conformation when bound to Erk2.

In summary, our structures provide new insights into the molecular basis for the rigorous substrate specificity of HePTP. We demonstrate a dual role for H237, which forms both an aromatic interaction with the phenyl ring of the substrate phosphotyrosine and a strong hydrogen bond (2.5 Å) with the main chain carbonyl of the substrate phosphotyrosine. This latter interaction functions to lock the flexible WPD loop over the substrate phosphotyrosine and optimally position WPD loop residue D236 for participation in catalysis. These structures also show that K105, in contrast to its equivalent residue in PTP1B, does not play a central role in substrate binding as its side chain is either disordered or, when ordered, does not interact with the substrate peptide. These structures also illustrate why monophosphorylated (*p*Y) and dually phosphorylated (*p*T*p*Y) Erk2 are dephosphorylated by HePTP with similar catalytic efficiencies: the side chains of Erk2 peptide residue T183 and the phospho-threonine mimic *D*183 do not interact with HePTP and thus do not contribute to binding. Finally, these structures demonstrate the importance of residue T106 in restraining promiscuous substrate binding; the HePTP KIM offsets this restraint by increasing the local concentration of highly specific substrates (e.g., Erk and p38). This complementary, 2-fold regulation of substrate binding is expected to characterize not only HePTP but all members of the KIM-phosphatase family.

ACKNOWLEDGMENT

SUPPORTING INFORMATION AVAILABLE

Additional details describing structure determination, biophysical characterization, and structural analysis of substrate-trapping mutants examined in this study. This

material is available free of charge via the Internet at http://pubs.acs.org.

REFERENCES

1. Hunter, T., and Sefton, B. M. (1980) Transforming gene product of Rous sarcoma virus phosphorylates tyrosine. *Proc. Natl. Acad. Sci. U.S.A. 77*, 1311–1315.

2. Alonso, A., Sasin, J., Bottini, N., Friedberg, I., Osterman, A., Godzik, A., Hunter, T., Dixon, J., and Mustelin, T. (2004) Protein tyrosine phosphatases in the human genome. *Cell 117*, 699–711.

3. Andersen, J. N., Jansen, P. G., Echwald, S. M., Mortensen, O. H., Fukada, T., Del Vecchio, R., Tonks, N. K., and Moller, N. P. (2004) A genomic perspective on protein tyrosine phosphatases: gene structure, pseudogenes, and genetic disease linkage. *FASEB J. 18*, 8–30.

4. Ostman, A., Hellberg, C., and Bohmer, F. D. (2006) Protein-tyrosine phosphatases and cancer. *Nat. Rev. Cancer 6*, 307–320.

5. Adachi, M., Sekiya, M., Isobe, M., Kumura, Y., Ogita, Z., Hinoda, Y., Imai, K., and Yachi, A. (1992) Molecular cloning and chromosomal mapping of a human protein-tyrosine phosphatase LC-PTP. *Biochem. Biophys. Res. Commun. 186*, 1607–1615.

6. Zanke, B., Suzuki, H., Kishihara, K., Mizzen, L., Minden, M., Pawson, A., and Mak, T. W. (1992) Cloning and expression of an inducible lymphoid-specific, protein tyrosine phosphatase (HeP-TPase). *Eur. J. Immunol. 22*, 235–239.

7. Gjorloff-Wingren, A., Saxena, M., Han, S., Wang, X., Alonso, A., Renedo, M., Oh, P., Williams, S., Schnitzer, J., and Mustelin, T. (2000) Subcellular localization of intracellular protein tyrosine phosphatases in T cells. *Eur. J. Immunol. 30*, 2412–2421.

8. Saxena, M., Williams, S., Gilman, J., and Mustelin, T. (1998) Negative regulation of T cell antigen receptor signal transduction by hematopoietic tyrosine phosphatase (HePTP). *J. Biol. Chem. 273*, 15340–15344.

9. Gronda, M., Arab, S., Iafrate, B., Suzuki, H., and Zanke, B. W. (2001) Hematopoietic protein tyrosine phosphatase suppresses extracellular stimulus-regulated kinase activation. *Mol. Cell. Biol. 21*, 6851–6858.

10. Munoz, J. J., Tarrega, C., Blanco-Aparicio, C., and Pulido, R. (2003) Differential interaction of the tyrosine phosphatases PTP-SL, STEP and HePTP with the mitogen-activated protein kinases ERK1/2 and p38alpha is determined by a kinase specificity sequence and influenced by reducing agents. *Biochem. J. 372*, 193–201.

11. Pettiford, S. M., and Herbst, R. (2000) The MAP-kinase ERK2 is a specific substrate of the protein tyrosine phosphatase HePTP. *Oncogene 19*, 858–869.

12. Saxena, M., Williams, S., Brockdorff, J., Gilman, J., and Mustelin, T. (1999) Inhibition of T cell signaling by mitogen-activated protein kinase-targeted hematopoietic tyrosine phosphatase (HePTP). *J. Biol. Chem. 274*, 11693–11700.

13. Andersen, J. N., Mortensen, O. H., Peters, G. H., Drake, P. G., Iversen, L. F., Olsen, O. H., Jansen, P. G., Andersen, H. S., Tonks, N. K., and Moller, N. P. (2001) Structural and evolutionary relationships among protein tyrosine phosphatase domains. *Mol. Cell. Biol. 21*, 7117–7136.

14. Eswaran, J., von Kries, J. P., Marsden, B., Longman, E., Debreczeni, J. E., Ugochukwu, E., Turnbull, A., Lee, W. H., Knapp, S., and Barr, A. J. (2006) Crystal structures and inhibitor identification for PTPN5, PTPRR and PTPN7: a family of human MAPK-specific protein tyrosine phosphatases. *Biochem. J. 395*, 483–491.

15. Mustelin, T., Tautz, L., and Page, R. (2005) Structure of the hematopoietic tyrosine phosphatase (HePTP) catalytic domain: structure of a KIM phosphatase with phosphate bound at the active site. *J. Mol. Biol. 354*, 150–163.

16. Lesley, S. A., Kuhn, P., Godzik, A., Deacon, A. M., Mathews, I., Kreusch, A., Spraggon, G., Klock, H. E., McMullan, D., Shin, T., Vincent, J., Robb, A., Brinen, L. S., Miller, M. D., McPhillips, T. M., Miller, M. A., Scheibe, D., Canaves, J. M., Guda, C., Jaroszewski, L., Selby, T. L., Elsliger, M. A., Wooley, J., Taylor, S. S., Hodgson, K. O., Wilson, I. A., Schultz, P. G., and Stevens, R. C. (2002) Structural genomics of the *Thermotoga maritima* proteome implemented in a high-throughput structure determination pipeline. *Proc. Natl. Acad. Sci. U.S.A. 99*, 11664–11669.

17. Peti, W., and Page, R. (2007) Strategies to maximize heterologous protein expression in *Escherichia coli* with minimal cost. *Protein Expression Purif. 51*, 1–10.

18. Zhang, F., Robbins, D. J., Cobb, M. H., and Goldsmith, E. J. (1993) Crystallization and preliminary X-ray studies of extracellular signal-regulated kinase-2/MAP kinase with an incorporated His-tag. *J. Mol. Biol. 233*, 550–552.

19. Pervushin, K., Riek, R., Wider, G., and Wuthrich, K. (1997) Attenuated T2 relaxation by mutual cancellation of dipole-dipole coupling and chemical shift anisotropy indicates an avenue to NMR structures of very large biological macromolecules in solution. *Proc. Natl. Acad. Sci. U.S.A. 94*, 12366–12371.

20. Otwinowski, Z., and Minor, W. (1997) Processing of X-ray diffraction data collected in oscillation mode. *Methods Enzymol. (Part A) 276*, 307–326.

21. McCoy, A. J., Grosse-Kunstleve, R. W., Storoni, L. C., and Read, R. J. (2005) Likelihood-enhanced fast translation functions. *Acta Crystallogr., Sect. D: Biol. Crystallogr. 61*, 458–464.

22. Emsley, P., and Cowtan, K. (2004) Coot: model-building tools for molecular graphics. *Acta Crystallogr., Sect. D: Biol. Crystallogr. 60*, 2126–2132.

23. Murshudov, G. N., Vagin, A. A., and Dodson, E. J. (1997) Refinement of macromolecular structures by the maximum-likelihood method. *Acta Crystallogr., Sect. D: Biol. Crystallogr. 53*, 240–255.

24. Lovell, S. C., Davis, I. W., Arendall, W. B., III, de Bakker, P. I., Word, J. M., Prisant, M. G., Richardson, J. S., and Richardson, D. C. (2003) Structure validation by Calpha geometry: phi,psi and Cbeta deviation. *Proteins 50*, 437–450.

25. Vaguine, A. A., Richelle, J., and Wodak, S. J. (1999) SFCHECK: a unified set of procedures for evaluating the quality of macromolecular structure-factor data and their agreement with the atomic model. *Acta Crystallogr. D 55*, 191–205.

26. Huang, Z., Zhou, B., and Zhang, Z. Y. (2004) Molecular determinants of substrate recognition in hematopoietic protein-tyrosine phosphatase. *J. Biol. Chem. 279*, 52150–52159.

27. Xie, L., Zhang, Y. L., and Zhang, Z. Y. (2002) Design and characterization of an improved protein tyrosine phosphatase substrate-trapping mutant. *Biochemistry 41*, 4032–4039.

28. Robbins, D. J., Zhen, E., Owaki, H., Vanderbilt, C. A., Ebert, D., Geppert, T. D., and Cobb, M. H. (1993) Regulation and properties of extracellular signal-regulated protein kinases 1 and 2 in vitro. *J. Biol. Chem. 268*, 5097–5106.

29. Shen, K., Hines, A. C., Schwarzer, D., Pickin, K. A., and Cole, P. A. (2005) Protein kinase structure and function analysis with chemical tools. *Biochim. Biophys. Acta 1754*, 65–78.

30. Ivanov, M. I., Stuckey, J. A., Schubert, H. L., Saper, M. A., and Bliska, J. B. (2005) Two substrate-targeting sites in the *Yersinia* protein tyrosine phosphatase co-operate to promote bacterial virulence. *Mol. Microbiol. 55*, 1346–1356.

31. Jia, Z., Barford, D., Flint, A. J., and Tonks, N. K. (1995) Structural basis for phosphotyrosine peptide recognition by protein tyrosine phosphatase 1B. *Science 268*, 1754–1758.

32. Salmeen, A., Andersen, J. N., Myers, M. P., Tonks, N. K., and Barford, D. (2000) Molecular basis for the dephosphorylation of the activation segment of the insulin receptor by protein tyrosine phosphatase 1B. *Mol. Cell 6*, 1401–1412.

33. Sarmiento, M., Puius, Y. A., Vetter, S. W., Keng, Y. F., Wu, L., Zhao, Y., Lawrence, D. S., Almo, S. C., and Zhang, Z. Y. (2000) Structural basis of plasticity in protein tyrosine phosphatase 1B substrate recognition. *Biochemistry 39*, 8171–8179.

34. Schumacher, M. A., Todd, J. L., Rice, A. E., Tanner, K. G., and Denu, J. M. (2002) Structural basis for the recognition of a bisphosphorylated MAP kinase peptide by human VHR protein phosphatase. *Biochemistry 41*, 3009–3017.

35. Brocchieri, L., and Karlin, S. (1994) Geometry of interplanar residue contacts in protein structures. *Proc. Natl. Acad. Sci. U.S.A. 91*, 9297–9301.

36. Burley, S. K., and Petsko, G. A. (1985) Aromatic-aromatic interaction: a mechanism of protein structure stabilization. *Science 229*, 23–28.

37. McGaughey, G. B., Gagne, M., and Rappe, A. K. (1998) pi-Stacking interactions. Alive and well in proteins. *J. Biol. Chem. 273*, 15458–15463.

38. Mitchell, J. B., Laskowski, R. A., and Thornton, J. M. (1997) Non-randomness in side-chain packing: the distribution of interplanar angles. *Proteins 29*, 370–380.

39. Thomas, A., Meurisse, R., Charloteaux, B., and Brasseur, R. (2002) Aromatic side-chain interactions in proteins. I. Main structural features. *Proteins 48*, 628–634.

40. Szedlacsek, S. E., Aricescu, A. R., Fulga, T. A., Renault, L., and Scheidig, A. J. (2001) Crystal structure of PTP-SL/PTPBR7

catalytic domain: implications for MAP kinase regulation. *J. Mol. Biol. 311*, 557–568.

41. Yang, J., Cheng, Z., Niu, T., Liang, X., Zhao, Z. J., and Zhou, G. W. (2000) Structural basis for substrate specificity of protein-tyrosine phosphatase SHP-1. *J. Biol. Chem. 275*, 4066–4071.

42. Kennelly, P. J., and Krebs, E. G. (1991) Consensus sequences as substrate specificity determinants for protein kinases and protein phosphatases. *J. Biol. Chem. 266*, 15555–15558.

43. Nika, K., Charvet, C., Williams, S., Tautz, L., Bruckner, S., Rahmouni, S., Bottini, N., Schoenberger, S. P., Baier, G., Altman, A., and Mustelin, T. (2006) Lipid raft targeting of hematopoietic protein tyrosine phosphatase by protein kinase C theta-mediated phosphorylation. *Mol. Cell. Biol. 26*, 1806–1816.

44. Nika, K., Hyunh, H., Williams, S., Paul, S., Bottini, N., Tasken, K., Lombroso, P. J., and Mustelin, T. (2004) Haematopoietic protein tyrosine phosphatase (HePTP) phosphorylation by cAMP-dependent protein kinase in T-cells: dynamics and subcellular location. *Biochem. J. 378*, 335–342.

45. Zhou, T., Sun, L., Humphreys, J., and Goldsmith, E. J. (2006) Docking interactions induce exposure of activation loop in the MAP kinase ERK2. *Structure 14*, 1011–1019.

46. Canagarajah, B. J., Khokhlatchev, A., Cobb, M. H., and Goldsmith, E. J. (1997) Activation mechanism of the MAP kinase ERK2 by dual phosphorylation. *Cell 90*, 859–869.

47. DeLano, W. L. (2002) The PyMOL Molecular Graphics System, DeLano Scientific, Palo Alto, CA.

48. Wallace, A. C., Laskowski, R. A., and Thornton, J. M. (1995) LIGPLOT: a program to generate schematic diagrams of protein-ligand interactions. *Protein Eng. 8*, 127–134.